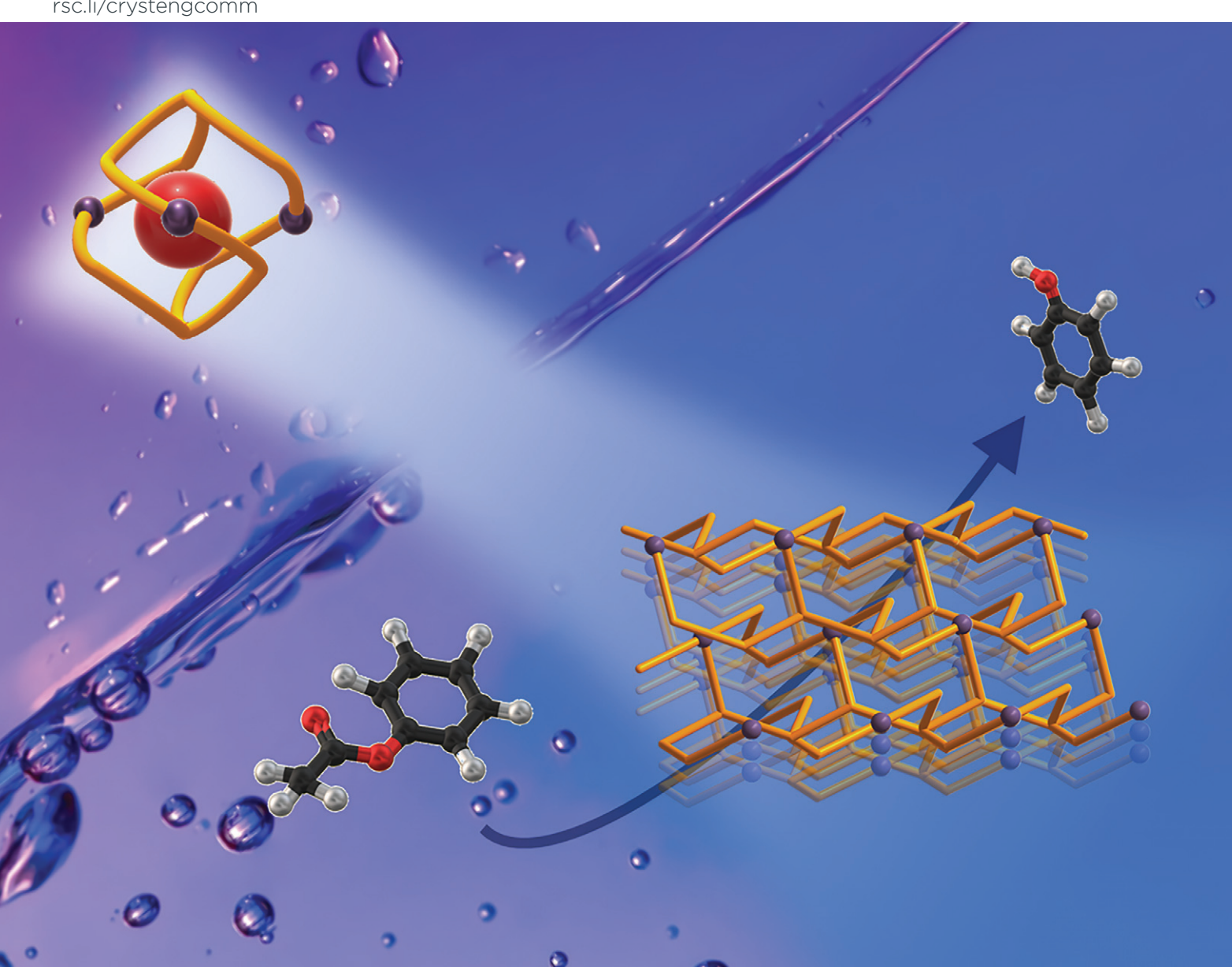
Volume 26 Number 7 21 February 2024 Pages 889-1040

CrystEngComm

rsc.li/crystengcomm



ISSN 1466-8033



PAPER

Ok-Sang Jung et al. Construction and catalytic effects of solvent- and metal(II)-dependent products: the process of transformation of OD structures into 3D structures

CrystEngComm



PAPER

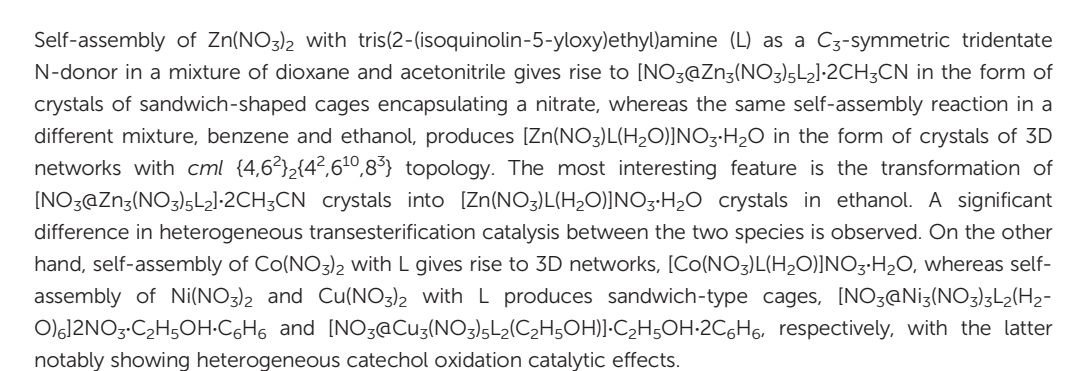
View Article Online



Cite this: CrystEngComm, 2024, 26, 918

Construction and catalytic effects of solvent- and metal(II)-dependent products: the process of transformation of 0D structures into 3D structures†

Gyeongmin Kim, Jihun Han, Dongwon Kim and Ok-Sang Jung **D**



Received 21st December 2023, Accepted 14th January 2024

DOI: 10.1039/d3ce01298k

rsc.li/crystengcomm

Introduction

Construction of diverse coordination architectures combinations of metal cations and spacer donors and its geometric principle have beckoned chemists over the past decade, 1-10 especially after the discovery of practical task-specific functions. If the coordination components of metal cations and spacer donors could be desirably assembled, what would both the resultant structures and the applications of their assembled products be? Discovery of a methodology for synthesis of various coordination architectures via deliberate driving forces is a significant challenge, and not concomitantly, is also an intriguing idea in the area of coordination materials.11-18 A prerequisite to the development of diverse coordination materials is the comprehension of the substantial driving forces behind the formation of different coordination networks for the same components. Furthermore, the process of interconversion between two different coordination assemblies from the same

Department of Chemistry, Pusan National University, Busan 46241, Republic of Korea. E-mail: oksjung@pusan.ac.kr; Fax: +82 51 5163522; Tel: +82 51 5103240 † Electronic supplementary information (ESI) available: Experimental details and crystal structure determination. TG curves, IR spectra, and ¹H NMR of each $sample \quad \hbox{$([Zn(NO_3)L(H_2O)](NO_3)$-$H_2O$, $ [NO_3@Zn_3(NO_3)_5L_2]$-$2CH_3CN$, $ [Co(NO_3)]$-$1.00 and $1.00 a$ $L(H_2O)](NO_3)\cdot H_2O$, $[NO_3@Ni_3(NO_3)_3L_2(H_2O)_6]2NO_3\cdot C_2H_5OH\cdot C_6H_6,$ $[NO_3 @ Cu_3 (NO_3)_5 L_2 (C_2 H_5 O H)] \cdot C_2 H_5 O H \cdot 2 C_6 H_6). \ \ CCDC \ \ 2320515 - 2320519. \ \ For \ ESI$ and crystallographic data in CIF or other electronic format see DOI: https://doi. org/10.1039/d3ce01298k

components is a fascinating research topic relevant to developments in efficient adsorption/desorption, molecular recognition, anion exchange, and catalysis. 19-24 Thus, rich data on the geometry of metal cations with the binding sites, lengths, and flexibility of multidentate donors in mixture solvent systems might afford new avenues to efficient coordination materials. Indeed, the combination of first-row transition metal cations and flexible multidentate N-donors suggests such a route.²⁵ In this context, the two ambitious aims of the present article were to explore the transformation process between two different coordination species via both photoluminescence (PL) spectra and time-dependent morphology change, and to investigate the solvent and metal cation effects on the self-assembly of first-row transition M2+ cations with a new flexible tridentate donor. Additionally, heterogeneous catalysis reactions using the present coordination species, namely zinc(II) and copper(II), were attempted. These coordination species have been known to be useful in the transesterification of a wide range of esters with alcohols and the oxidation of various alcohols, respectively. In particular, zinc(II) species have been investigated and deemed to be useful metal cations for Lewis acids, metallo-enzymes, zinc finger proteins, and PL materials.26-31

Experimental

Reagents and measurement

All of the chemicals including $M(NO_3)_2$ (M(II) = Zn(II), Co(II), $Ni(\Pi)$, and $Cu(\Pi)$) were purchased from Aldrich and used

CrystEngComm Paper

without further purification. ¹H NMR spectra were recorded on a Varian Mercury Plus 400 instrument operating at 400 MHz. Infrared spectra were obtained on a Nicolet 380 FT-IR spectrophotometer with samples prepared as KBr pellets. Elemental microanalyses (C, H, N) were performed on solid samples at the Pusan Center, KBSI, using a Vario-EL III. Thermal analyses were carried out under a dinitrogen atmosphere at a scan rate of 10 °C min⁻¹ using a Labsys TGA-DSC 1600. Excitation and emission spectra were recorded on a Hitachi F-7000 spectrofluorometer.

Synthesis of tris(2-(isoquinolin-5-yloxy)ethyl)amine

Triethanolamine (3.96 mL, 30.0 mmol) was slowly added to a solution of stirred thionyl chloride (4.4 mL, 60.0 mmol) in chloroform (20 mL), and the mixture was further stirred at 25 °C for 1 h. Evaporation of the chloroform solution afforded a white solid, tris(2-chloroethyl)amine, in a 99.4% yield (6.1 g). The dried tris(2-chloroethyl)amine (2.4 g, 10.0 mmol) was slowly added to a mixture of 5-hydroxyisoquinoline (4.8 g, 33.3 mmol) and sodium hydroxide (2.0 g, 50.0 mmol) in ethanol (100.0 mL), and the reactant mixture was refluxed at 80 °C for 8 h. Evaporation of the ethanol solution afforded a red liquid. Then, the chloroform solution of the liquid product was washed with aqueous NaOH solution several times, and the chloroform layer was dried over anhydrous sodium sulfate. The pink solid obtained by evaporation of chloroform was purified by column chromatography on silica gel (dichloromethane: ethyl acetate: hexane = 80:15:5 volumes as eluent) to obtain the product in a 76.0% yield. m. p. 150 °C (dec.). Anal. Calcd. for C₃₃H₃₀N₄O₃: C, 74.70; H, 5.70; N, 10.56%. Found: C, 74.40; H, 5.52; N, 10.28%. IR (KBr pellet, cm⁻¹): 3055(w), 2925(m), 2866(w), 1628(w), 1582(s), 1492(s), 1458(m), 1438(s), 1393(s), 1365(s), 1323(s), 1278(s), 1255(s), 1217(m), 1178(m), 1117(m), 1062(m), 1020(m), 943(w), 916(m), 829(s), 803(m), 750(s), 649(w), 580(w), 446(w), 408(w). 1 H NMR (in Me₂SO- d_{6} , δ): 9.20 (s, 3H), 8.10 (d, J =5.75 Hz, 3H), 7.79 (d, J = 5.88 Hz, 3H), 7.60 (d, J = 8.25 Hz, 6H), 7.53 (t, J = 7.94 Hz, 3H), 7.20 (d, J = 7.63 Hz, 3H), 4.36 (t, J = 5.31 Hz, 6H, 3.34 (t, <math>J = 5.38 Hz, 6H).

$[Zn(NO_3)L(H_2O)]NO_3 \cdot H_2O$

An ethanol solution (4.0 mL) of zinc(II) nitrate hexahydrate (3.6 mg, 0.012 mmol) was carefully layered onto a benzene solution (4.0 mL) of L (6.4 mg, 0.012 mmol). After 3 days, colorless crystals suitable for single crystal X-ray crystallography were obtained in an 85% yield. m.p. 218 °C (dec.). Anal. Calcd. for C₃₃H₃₄ZnN₆O₁₄: C, 49.30; H, 4.26; N, 10.45%. Found: C, 48.90; H, 4.30; N, 11.10%. IR (KBr pellet, cm^{-1}): 3065(w), 2945(w), 2817(w), 1631(w), 1595(m), 1499(s), 1445(m), 1441(m), 1384(s), 1280(s), 1255(m), 1221(m), 1185(m), 1117(m), 1069(w), 1041(m), 927(m), 837(m), 809(m), 751(m), 644(w), 584(w), 545(w), 473(w), 415(w). ¹H NMR (dissociated in Me₂SO- d_6 , δ): 9.20 (s, 3H), 8.10 (d, J = 5.75 Hz, 3H), 7.79 (d, J = 5.88 Hz, 3H), 7.60 (d, J = 8.25 Hz, 6H), 7.53 (t, J = 7.94 Hz, 3H), 7.20 (d, J = 7.63 Hz, 3H), 4.36 (t, J = 5.31)Hz, 6H), 3.34 (t, J = 5.38 Hz, 6H).

$[NO_3@Zn_3(NO_3)_5L_2] \cdot 2CH_3CN$

An acetonitrile solution (4.0 mL) of zinc(II) nitrate hexahydrate (3.6 mg, 0.012 mmol) was carefully layered onto a dioxane solution (4.0 mL) of L (6.4 mg, 0.012 mmol). After 4 days, colorless crystals suitable for single crystal X-ray crystallography were obtained in an 84% yield. m.p. 150 °C (dec.). Anal. Calcd. For C₇₀H₆₆Zn₃N₁₆O₂₄: C, 49.12; H, 3.89; N, 13.09%. Found: C, 49.20; H, 3.71; N, 13.10%. IR (KBr pellet, cm⁻¹): 3055(w), 2964(m), 2930(w), 1628(w), 1600(m), 1497(s), 1464(m), 1443(m), 1382(s), 1283(s), 1255(m), 1185(m), 1121(m), 1079(w), 1044(m), 929(m), 833(m), 803(m), 759(m), 646(w), 582(w), 540(w), 479(w), 418(w). ¹H NMR (dissociated in Me₂SO- d_6 , δ): 9.20 (s, 3H), 8.10 (d, J = 5.75 Hz, 3H), 7.79 (d, J = 5.88 Hz, 3H), 7.60 (d, J = 8.25 Hz, 6H), 7.53 (t, J = 7.94 Hz, 3H), 7.20 (d, J = 7.63 Hz, 3H), 4.36 (t, J = 5.31 Hz, 6H), 3.34 (t, I = 5.38 Hz, 6H).

[Co(NO₃)L(H₂O)]NO₃·H₂O

An ethanol solution (4.0 mL) of cobalt(II) nitrate hexahydrate (3.5 mg, 0.012 mmol) was carefully layered onto a benzene solution (4.0 mL) of L (6.4 mg, 0.012 mmol). After 2 days, white crystals suitable for single crystal X-ray crystallography were obtained in a 92% yield. m.p. 225 °C (dec.). Anal. Calcd. for C₃₃H₃₄CoN₆O₁₄: C, 49.69; H, 4.30; N, 10.54%. Found: C, 46.40; H, 4.32; N, 10.60%. IR (KBr pellet, cm⁻¹): 3444(s), 2947(w), 2813(w), 1633(m), 1598(s), 1499(m), 1475(m), 1439(m), 1387(s), 1326(w), 1285(s), 1259(w), 1211(w), 1181(w), 1116(m), 1042(m), 922(w), 833(m), 809(m), 747(m), 650(w), 547(w), 484(w). ¹H NMR (dissociated in Me₂SO- d_6 , δ): 9.20 (s, 3H), 8.10 (d, J = 5.75 Hz, 3H), 7.79 (d, J = 5.88 Hz, 3H), 7.60 (d, J = 8.25 Hz, 6H), 7.53 (t, J = 7.94 Hz, 3H), 7.20 (d, J = 7.63)Hz, 3H), 4.36 (t, J = 5.31 Hz, 6H), 3.34 (t, J = 5.38 Hz, 6H).

$[NO_3@Ni_3(NO_3)_3L_2(H_2O)_6]2NO_3\cdot C_2H_5OH\cdot C_6H_6$

An ethanol solution (4.0 mL) of nickel(II) nitrate hexahydrate (3.5 mg, 0.012 mmol) was carefully layered onto a benzene solution (4.0 mL) of L (6.4 mg, 0.012 mmol). After 2 days, white crystals suitable for single crystal X-ray crystallography were obtained in a 78% yield. m.p. 235 °C (dec.). Anal. Calcd. for C₇₄H₈₄Ni₃N₁₄O₃₁: C, 48.26; H, 4.60; N, 10.65%. Found: C, 48.10; H, 4.15; N, 10.20%. IR (KBr pellet, cm⁻¹): 3385(s), 2944(w), 2814(w), 1631(m), 1599(m), 1498(m), 1476(m), 1441(m), 1383(s), 1327(m), 1280(s), 1254(m), 1222(w), 1182(w), 1116(m), 1037(m), 1022(w), 922(w), 838(w), 808(w), 746(m), 6654(w), 535(w). 1 H NMR (dissociated in Me₂SO- d_6 , δ): 9.20 (s, 3H), 8.10 (d, J = 5.75 Hz, 3H), 7.79 (d, J = 5.88 Hz, 3H), 7.60 (d, J = 8.25 Hz, 6H), 7.53 (t, J = 7.94 Hz, 3H), 7.20 (d, J = 7.63 Hz, 3H), 4.36 (t, J = 5.31 Hz, 6H), 3.34 (t, J = 5.38)Hz, 6H).

Paper CrystEngComm

$[NO_3(a)Cu_3(NO_3)_5L_2(C_2H_5OH)]\cdot C_2H_5OH\cdot 2C_6H_6$

An ethanol solution (4.0 mL) of copper(II) nitrate hexahydrate (3.5 mg, 0.012 mmol) was carefully layered onto a benzene solution (4.0 mL) of L (6.4 mg, 0.012 mmol). After 7 days, blue crystals suitable for single crystal X-ray crystallography were obtained in an 88% yield. m.p. 239 °C (dec.). Anal. Calcd. for $C_{82}H_{84}Cu_3N_{14}O_{26}$: C, 52.60; H, 4.52; N, 10.48%. Found: C, 51.90; H, 4.48; N, 10.23%. IR (KBr pellet, cm⁻¹): 3485(s), 2379(w), 2344(w), 1650(m), 1595(m), 1390(s), 1286(w), 1187(w), 1120(w), 1051(w), 841(w), 757(w), 650(w), 531(w).

Transformation of [NO₃@Zn₃(NO₃)₅L₂]·2CH₃CN into $[Zn(NO_3)L(H_2O)]NO_3 \cdot H_2O$

Single crystals of [NO₃@Zn₃(NO₃)₅L₂]·2CH₃CN (0.003 mmol) left in 1.5 mL of 95% ethanol resulted in the formation of [Zn(NO₃)L(H₂O)]NO₃·H₂O in a 70% yield (based on Zn(II)) after 1 day.

Transesterification catalysis

The zinc(II) catalysts were employed as catalysts for the transesterification reaction of phenyl acetate with methanol. Each zinc(II) catalyst (80, 172 mg, 0.1 mmol) and phenyl acetate (0.13 mL, 1.0 mmol) were stirred in methanol (10 mL), and heated up to 40 °C. The catalytic process was monitored by referring to the ¹H NMR spectra.

Catechol oxidation catalysis

3,5-Di-tert-butylcatechol (3,5-DBuCat) was employed as the substrate for catalytic oxidation reactions. The present copper(II) catalysts (18.7 mg, 0.01 mmol) were treated with the substrate (22.3 mg, 0.1 mmol) in acetone (10 mL) at 40 °C under aerobic conditions. The catalytic yields were monitored by referring to the UV-vis and ¹H NMR spectra.

Single crystal X-ray crystallography

All of the X-ray diffraction data (except for [NO₃@Cu₃(NO₃)₅- $L_2(C_2H_5OH)]\cdot C_2H_5OH\cdot 2C_6H_6$) were measured at 153 K or 223 K with synchrotron radiation ($\lambda = 0.63000 - 0.70000 \text{ Å}$) on a Rayonix MX225HS detector at 2D SMC with a silicon (111) double-crystal monochromator (DCM) at the Pohang Accelerator Laboratory, Korea. The PAL BL2D-SMDC program³² was used for data collection (detector distance: 66 mm, omega scan: $\Delta \omega = 3^{\circ}$, exposure time: 1 s per frame), and HKL3000sm (ver. 703r)33 was used for cell refinement, reduction, and absorption correction. X-ray data on $[NO_3@Cu_3(NO_3)_5L_2(C_2H_5OH)]\cdot C_2H_5OH\cdot 2C_6H_6$ were collected on a Bruker SMART automatic diffractometer with graphitemonochromated Mo K α radiation ($\lambda = 0.71073$ Å). Thirty-six (36) frames of 2D diffraction images were collected and processed to obtain the cell parameters and orientation matrix. The data were corrected for Lorentz and polarization effects. The absorption effects were corrected using the multi-scan method (SADABS).34 The structures were solved using the direct method (SHELXS) and refined by a fullmatrix least squares technique (SHELXL 2018/3).35 The nonhydrogen atoms were refined anisotropically, and the hydrogen atoms were placed in calculated positions and refined only for the isotropic thermal factors. For only $[NO_3@Ni_3(NO_3)_3L_2(H_2O)_6]2NO_3\cdot C_2H_5OH\cdot C_6H_6$, two nitrates, one ethanol and one benzene solvate were squeezed by using the SQUEEZE routine in PLATON.³⁶ The crystal parameters and procedural information corresponding to the data collection and structure refinement are listed in Tables S1 and S2.†

Results and discussion

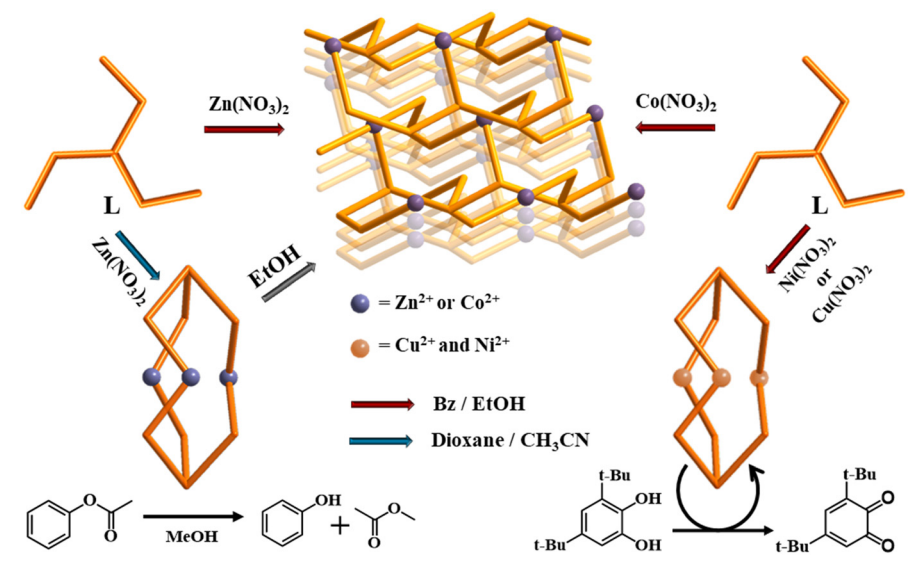
Synthesis

The new flexible tridentate ligand, tris(2-(isoquinolin-5-yloxy) ethyl)amine (L), was synthesized by the reaction of tris(2chloroethyl)amine with 5-hydroxyisoquinoline in a high yield. As shown in Scheme 1, the self-assembly of Zn(NO₃)₂ in acetonitrile with L in dioxane produced colorless crystals consisting of discrete cages encapsulating a nitrate, [NO₃@Zn₃(NO₃)₅L₂]·2CH₃CN, whereas the self-assembly in a different mixture of ethanol and benzene afforded crystals of networks, $[Zn(NO_3)L(H_2O)]NO_3\cdot H_2O.$ confirmed the self-assembly reactions to have been strongly dependent on the reaction solvents. Moreover, the crystals consisting of cages, [NO₃@Zn₃(NO₃)₅L₂]-2CH₃CN, were left in ethanol, and transformed into [Zn(NO3)L(H2O)]NO3·H2O in the form of crystals of 3D networks after 1 day. On the other hand, the self-assembly of Co(NO₃)₂ with L gave rise to [Co(NO₃)L(H₂O)]NO₃·H₂O in the form of crystals of 3D networks, whereas the self-assembly reactions of Ni(NO₃)₂ and Cu(NO₃)₂ with L in the same solvent mixture produced $[NO_3@Ni_3(NO_3)_3L_2(H_2O)_6]2NO_3\cdot C_2H_5OH\cdot C_6H_6$ $[NO_3@Cu_3(NO_3)_5L_2(C_2H_5OH)]\cdot C_2H_5OH\cdot 2C_6H_6$, respectively, in the form of discrete cages, indicating that such self-assembly reactions exhibit metal(II) ion effects. The self-assembly reactions were originally carried out at the mole ratio of 1:1, but the formation of the products was not significantly affected by the change of the reactant mole ratio or concentration. All of the species are insoluble in water, chloroform, acetone, and dichloromethane, but are easily dissociated in polar organic solvents such as dimethyl sulfoxide and N,N-dimethylformamide. [NO₃@Zn₃(NO₃)₅-L₂]·2CH₃CN is slowly dissociated in ethanol. The compositions and structures of all of the products were confirmed by elemental analyses, ¹H NMR (Fig. S1†), IR (Fig. S2†), thermal analysis (Fig. S3†), and single crystal X-ray diffraction. Thermogravimetric analysis indicated that $[NO_3@Zn_3(NO_3)_5L_2]\cdot 2CH_3CN$ and $[Zn(NO_3)L(H_2O)]NO_3\cdot H_2O$ were stable up to 260 and 270 °C, respectively. Their solvate acetonitrile molecules and water molecules were evaporated at 145-180 and 50-80 °C, respectively.

Crystal structures

The X-ray single-crystal characterization provided discrete cages or 3D networks depending on the solvents and

CrystEngComm Paper



Scheme 1 Overall synthesis including dimensional transformation and catalysis of M₃L₂ cages into 3D networks.

transition metal(II) cations (Scheme 1 and Fig. 1 and 2), and the relevant bond distances and angles are listed in Table 1. For [NO₃@Zn₃(NO₃)₅L₂]·2CH₃CN, L is connected to three Zn(II) ions (Zn-N = 2.001(4)-2.054(3) Å) in a tridentate fashion to form a discrete sandwich-type Zn₃L₂ cage with a Zn···Zn separation of 5.258(2)-5.887(1) Å. The local geometries around the three zinc(II) ions correspond to three different six-to-seven coordination arrangements with two N donors from two Ls and four-to-five O donors from nitrate anions (Zn-O = 1.999(7)-2.071(7) Å). One nitrate is encapsulated inside the cage and interacts with three Zn(II) ions. Acetonitrile solvates are positioned in the vacancy of the inter-cage. The shortest inter-cage distance is O(NO₃) \cdots O(NO₃) = 3.108(2) Å (see the structure (Fig. S4†) packed in abab... along the a-axis). The crystal structures of $[NO_3@Ni_3(NO_3)_3L_2(H_2O)_6]2NO_3\cdot C_2H_5OH\cdot C_6H_6$ $[NO_3@Cu_3(NO_3)_5L_2(C_2H_5OH)]\cdot C_2H_5OH\cdot 2C_6H_6$ are basically the same cage, though with a slightly different coordination geometry around each central metal cation. For each crystal, solvate molecules are positioned in the vacancy of

the inter-cages without any significant interactions. In contrast, the crystal structure of [Zn(NO₃)L(H₂O)]NO₃·H₂O shows that L is coordinated to three Zn(II) ions in a tridentate mode to produce a 3D network with cml $\{4,6^2\}_2\{4^2,6^{10},8^3\}$ topology, as depicted in Fig. 2 using the known program.37 The geometry around the Zn(II) cation is an octahedral arrangement with three N donors from three Ls and one bidentate nitrate and one water molecule. Both a nitrate counteranion and a water solvate molecule occupy the vacancy of the networks. The crystal structure of [Co(NO₃)L(H₂O)]NO₃·H₂O is the same 3D network. The conformations of L in the cages and the 3D networks are quite different: the L moiety of the cages and the 3D networks is in a tripodal and a triaxial fashion, respectively (Fig. S5†).

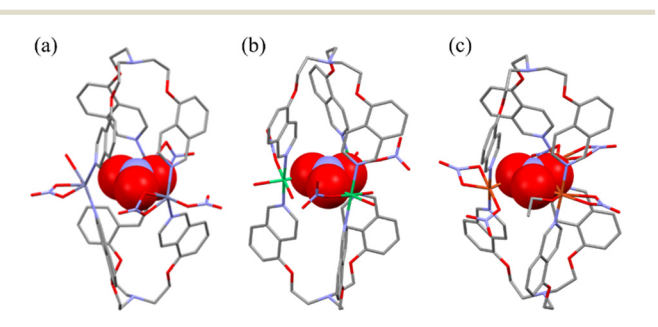


Fig. 1 Crystal structures of $[NO_3@Zn_3(NO_3)_5L_2]\cdot 2CH_3CN$ $[\mathsf{NO_3@Ni_3(NO_3)_3L_2(H_2O)_6}] \\ 2\mathsf{NO_3\cdot C_2H_5OH\cdot C_6H_6}$ (b). $[NO_3@Cu_3(NO_3)_5L_2(C_2H_5OH)] \cdot C_2H_5OH \cdot 2C_6H_6 \quad (c). \quad The \quad encapsulated$ nitrate anion is depicted in a space-filling mode: C (gray), O (red), N (sky blue), Zn (dark blue), Ni (green), and Cu (orange).

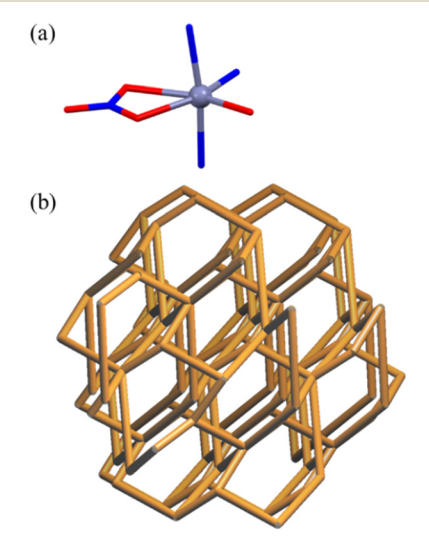


Fig. 2 Local geometry around M^{2+} (a) and 3D networks of $[Zn(NO_7)]$ $[Co(NO_3)L(H_2O)]NO_3 \cdot H_2O$ $L(H_2O)]NO_3 \cdot H_2O$ and with cml $\{4,6^2\}_2\{4^2,6^{10},8^3\}$ topology (b).

Paper

	$[NO_3 @Zn_3 (NO_3)_5 L_2] \cdot 2CH_3 CN$	$[NO_3@Ni_3(NO_3)_3L_2(H_2O)_6]2NO_3{\cdot}C_2H_5OH{\cdot}C_6H_6$	$[NO_3 @Cu_3 (NO_3)_5 L_2 (C_2 H_5 OH)] \cdot C_2 H_5 OH \cdot 2 C_6 H_6$
M-N (quinoline) (Å)	2.001(4)-2.054(3)	2.11(1)-2.131(4)	1.992(7)-2.024(8)
M-O (anion) (Å)	1.999(7)-2.071(7)	2.036(8)-2.16(1)	1.98(2)-2.256(9)
$\mathbf{M} \cdots \mathbf{M} \stackrel{\circ}{(A)}$	5.258(2)-5.887(1)	5.1759(8)	4.7543(4)-5.6949(5)
N-M-N (°)	120.5(2)-128.5(2)	177.3(3)	167.6(4)-178.3(3)

N-M-N (°)	120.5(2)-128.5(2)	177.3(3)	167.6(4)–178.3(3)
		$[Zn(NO_3)L(H_2O)](NO_3){\cdot}H_2O$	$[\mathrm{Co(NO_3)L(H_2O)}](\mathrm{NO_3)} \cdot \mathrm{H_2O}$
M–N (quinoline) (A M–O (anion) (Å) M–O (H ₂ O) (Å)	Å)	2.091(3)-2.179(3) 2.206(3) 2.031(3)	2.103(3)-2.175(3) 2.197(3) 2.056(3)

Construction principle and transformation

Self-assembly of first-row transition metal(II) cations with the new flexible tridentate ligand, tris(2-(isoquinolin-5-yloxy) ethyl)amine (L), can principally construct 0D, 1D, 2D, and 3D coordination architectures. And in fact, in the present case, the self-assembly of Zn(NO₃)₂ with L afforded 0D cages and 3D networks depending on the solvents employed. In the polar solvent system of dioxane and acetonitrile, selfassembly gave rise to a discrete cage, Zn3L2, with an encapsulated nitrate anion, whereas in the mixture of benzene and ethanol, it produced 3D networks with cml $\{4,6^2\}_2\{4^2,6^{10},8^3\}$ topology, owing presumably to the solvation energy and solubility difference in the self-assembly of the d^{10} Zn(II) cation with the flexible tridentate L. That is, the flexible conformation of L can contribute to the formation of solvent-dependent structures. In particular, when the single crystals of [NO₃@Zn₃(NO₃)₅L₂]-2CH₃CN were immersed in ethanol, they were slowly dissociated. Thus, the original crystals began to slowly transform to form new thermodynamic crystals of [Zn(NO₃)L(H₂O)]NO₃·H₂O in 95% ethanol (Fig. 3). This is an unusual observation, in which the original crystals transformed easily into new and stable crystals, depending on the solvents. Upon the measurement of the solid photoluminescence (PL) spectra ($\lambda_{ex} = 315$ nm) of the two present zinc(II) species [NO₃@Zn₃(NO₃)₅L₂]·2CH₃CN and [Zn(NO₃)L(H₂O)]NO₃·H₂O, together with those of L, the

Table 1 Relevant distances (Å) and angles (°) for the five crystal structures

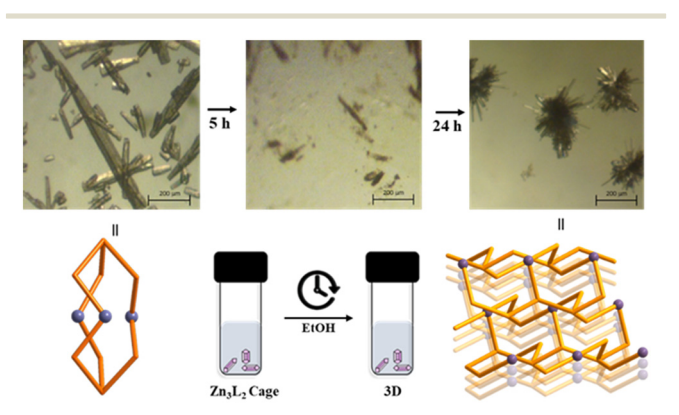


Fig. 3 Transformation process including morphology change of $[NO_3@Zn_3(NO_3)_5L_2]-2CH_3CN$ into $[Zn(NO_3)L(H_2O)]NO_3-H_2O$ in 95% ethanol

PL peaks of $[NO_3@Zn_3(NO_3)_5L_2]$ -2CH₃CN (λ_{max} = 435 nm) and $[Zn(NO_3)L(H_2O)]NO_3 \cdot H_2O$ ($\lambda_{max} = 405$ and 470 nm) were redshifted relative to the corresponding L (λ_{max} = 370 nm) (Fig. 4). The ligand's intrinsic characteristics play a pivotal role in the PL appearance of the two zinc(II) species. Indeed, these results suggest that the complexes' emission bands can be ascribed to the ligand-to-metal charge transfer (LMCT).38,39 Moreover, the transformation process of $[NO_3 \otimes Zn_3(NO_3)_5L_2] \cdot 2CH_3CN$ into $[Zn(NO_3)L(H_2O)]NO_3 \cdot H_2O$ could be confirmed by the PL spectra, as depicted in the figure: that is, when a drop of ethanol was placed on the crystals of [NO₃@Zn₃(NO₃)₅L₂]·2CH₃CN, the PL spectral change was in agreement with the aforementioned original solid PL spectrum of [Zn(NO₃)L(H₂O)]NO₃·H₂O. Formation of such solvent-dependent structures can be ascribed to both the d^{10} metal(II) cation (see the Irving-Williams series)⁴⁰ and the flexible tridentate L. The present self-assembly of Co(NO₃)₂ with L in a mixture of ethanol and benzene yielded the same 3D network, whereas that of Ni(NO₃)₂ and Cu(NO₃)₂ with L in the same solvent produced an M3L2 cage encapsulating a nitrate. That is, the two products are dependent on the M2+ cation. Thus, for Co(II), Ni(II), and

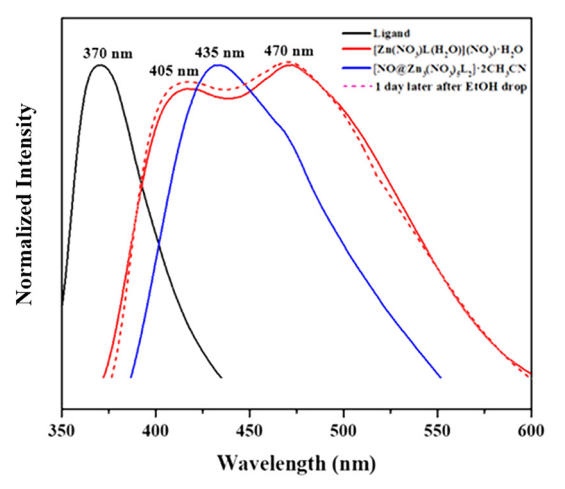


Fig. 4 PL spectra of L (black), $[NO_3@Zn_3(NO_3)_5L_2]\cdot 2CH_3CN$ (blue), and $[Zn(NO_3)L(H_2O)]NO_3 \cdot H_2O$ (red), and transformation $[NO_3@Zn_3(NO_3)_5L_2]\cdot 2CH_3CN$ into $[Zn(NO_3)L(H_2O)]NO_3\cdot H_2O$ (red dotted

CrystEngComm

Cu(II), the electronic structures, rather than the solvents employed, play an important role in the formation of products. This system with its flexible L affords delicate transition metal(II) effects in addition to strong solvent effects on the d^{10} metal cation in these self-assembly reactions.

Transesterification catalysis

Each Zn(II) catalyst (0.1 mmol) was dissolved in a mixture of methanol (10 mL) and phenyl acetate (0.13 mL, 1.0 mmol). The catalysis reactions were run at 40 °C for 10 h. The transesterification catalysis then converted phenyl acetate and methanol to phenol and methyl acetate. Their conversion yields were monitored by the corresponding ¹H NMR spectra (Fig. S6†). The catalysis using the 3D network, [Zn(NO₃) L(H₂O)]NO₃·H₂O, almost finished within 10 h, whereas the catalysis using the cage, [NO₃@Zn₃(NO₃)₅L₂]·2CH₃CN, had proceeded by only 14% for 10 h (Fig. 5). Thus, the two complexes show a significant difference in transesterification catalysis. Such contrasting catalytic activities can be explained by both the stability and structural differences between 3D and 0D under the catalysis conditions: that is, [NO₃@Zn₃(NO₃)₅L₂]·2CH₃CN is slowly dissociated in methanol. Thus, when a simple mixture of Zn(NO₃)₂ and L (1:1 mole ratio) was employed as a catalyst, the catalysis produced only about 17% yield for the same time. Such a fact is an interesting result that the transesterification reactions using both [NO₃@Zn₃(NO₃)₅L₂]·2CH₃CN and a simple mixture of Zn(NO₃)₂ and L (1:1 mole ratio) proceed homogeneously with dissociated catalytic species. Furthermore, when dried methanol was used in the catalysis reaction, the catalysis gave a similar pattern (Fig. S7†). However, the catalysis reaction in dried methanol was better than that in methanol including water. Such a fact is consistent with our previous results.41

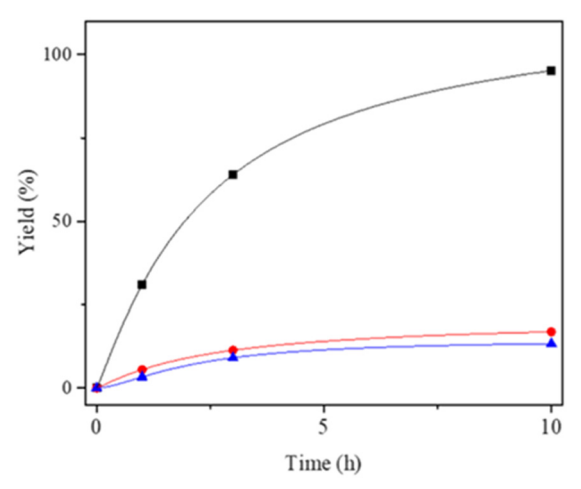


Fig. 5 Plots showing the transesterification catalysis of phenyl acetate with methanol using [Zn(NO₃)L(H₂O)](NO₃)·H₂O (black line), a mixture of $Zn(NO_3)_2:L$ (1:1) (red line), and $[NO_3@Zn_3(NO_3)_5L_2]\cdot 2CH_3CN$ (blue line) at 40 °C.

Catalysis of catechol oxidation

3,5-Di-tert-butylcatechol (3,5-DBCat) was employed as the substrate for the oxidation catalysis using the present copper(II) species. In particular, its oxidized form, 3,5-di-tertbutylquinone (3,5-DBBQ), is a potential non-innocent ligand for an intramolecular M-L electron transfer system, exhibiting a characteristic maximum absorption band at around 400 nm. 42-44 Thus, a heterogeneous catalytic oxidation reaction using [NO₃@Cu₃(NO₃)₅L₂(C₂H₅OH)]·C₂H₅-OH-2C₆H₆ was carried out. The catalyst was treated with 3,5-DBCat in the 1:10 mole ratio under aerobic conditions in 10 mL of acetone at 40 °C. After 3,5-DBCat and each catalyst were added to the acetone, the absorption band at 400 nm gradually increased in intensity. Thus, the relative reaction rates were monitored with reference to the increase in the UV band as a function of time (Fig. 6) along with the ¹H NMR spectra (Fig. S8†). The oxidation catalysis was completely finished within 180 min at room temperature. Moreover, it could be confirmed that the crystalline catalyst is more efficient than the mixture of Cu(NO₃)₂ and L. Additionally, the catalytic efficiency of the present cage crystals was compared relative to those of CuO, Cu(BF₄)₂, and Ag₂O.⁴⁰ The performance of the 1:100 (heterogeneous catalysts: substrate) mole catalyst has a negligible decrease, as depicted in the figure. After the reaction was completed, the mixture solution was centrifuged to recover the finely broken crystals. The IR and ¹H NMR spectra and PXRD patterns (Fig. S9†) indicated that the catalysts had maintained the skeletal structure after the heterogeneous catalytic reaction (Fig. S10†). The heterogeneous oxidation catalysis of the cage $[NO_3@Cu_3(NO_3)_5L_2(C_2H_5OH)]\cdot C_2H_5OH\cdot 2C_6H_6$ catalyst, seemed to arise from the existence of the appropriate intracage Cu···Cu distance (4.7543(4)-5.6949(5) Å), which is suitable for the coordination with catechol. 45

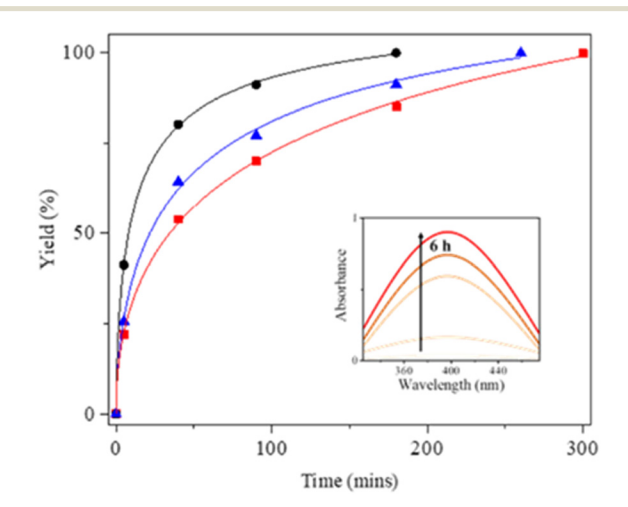


Fig. 6 Catalytic oxidation rates of 3,5-di-tert-butylcatechol (1 mmol) using [NO₃@Cu₃(NO₃)₅L₂(C₂H₅OH)]·C₂H₅OH·₂C₆H₆ dependent on the catalyst quantity: 0.1 mmol (black line), 0.05 mmol (blue line), and 0.01 mmol (red line), at 40 °C in 10 mL aceton.

Paper

Conclusions

Self-assembly of the d^{10} metal cation $Zn(NO_3)_2$ with tris(2-(isoquinolin-5-yloxy)ethyl)amine (L) as a flexible tridentate ligand yields a discrete sandwich-shaped cage encapsulating a nitrate, [Zn₃(NO₃)₆L₂]2CH₃CN, and 3D networks, [Zn(NO₃) L(H2O)](NO3)·H2O, depending on the solvents employed. This paper provides a proof of concept that the self-assembly of a d^{10} metal(II) cation with a flexible C_3 -symmetric tridentate ligand facilitates the formation of sandwich-shaped M₃L₂ architectures and 3D networks according to the polarity and shape of solvents. Further, an unusual transformation of $[NO_3@Zn_3(NO_3)_5L_2]\cdot 2CH_3CN$ into $[Zn(NO_3)L(H_2O)](NO_3)\cdot H_2O$ was observed. A similar self-assembly of Co(NO₃)₂ with L gave rise to 3D networks, whereas the self-assembly of Ni(NO₃)₂ or Cu(NO₃)₂ with L produced similar cages, indicating strong metal cation effects on the self-assembly. Different transesterification catalysis between the 0D cage and 3D network was observed, indicating that the structural features are key factors in catalysis. Upcoming experiments will provide more detailed information on the supramolecular ensemble's enormous potentials stemming from its catalytic-mechanistic, adsorption-desorption and photoluminescence properties.

Conflicts of interest

There are no conflicts to declare.

Acknowledgements

This work was supported by the National Research Foundation of Korea (NRF) grants funded by the Korean [MEST] (2021R1A2C2005105). Government crystallography at the PLS-II 2D-SMC beamline was supported in part by MSIP and POSTECH.

Notes and references

- 1 M. D. Allendorf, C. A. Bauer, R. Bhakta and R. Houk, Chem. Soc. Rev., 2009, 38, 1330-1352.
- 2 R. Chakrabarty, P. S. Mukherjee and P. J. Stang, Chem. Rev., 2011, 111, 6810-6918.
- 3 H. Furukawa, K. E. Cordova, M. O'Keeffe and O. M. Yaghi, Sci., 2013, 341, 1230444.
- 4 S. L. James, Chem. Soc. Rev., 2003, 32, 276-288.
- 5 C. Janiak, Dalton Trans., 2003, 2781-2804.
- 6 S. Kitagawa, R. Kitaura and S. I. Noro, Angew. Chem., Int. Ed., 2004, 43, 2334-2375.
- 7 W. P. Lustig, S. Mukherjee, N. D. Rudd, A. V. Desai, J. Li and S. K. Ghosh, Chem. Soc. Rev., 2017, 46, 3242-3285.
- 8 B. Moulton and M. J. Zaworotko, Chem. Rev., 2001, 101, 1629-1658.
- 9 P. Simon and Y. Gogotsi, Nat. Mater., 2008, 7, 845-854.
- 10 A. V. Desai, S. Sharma, S. Let and S. K. Ghosh, Coord. Chem. Rev., 2019, 395, 146-192.
- 11 H. Abourahma, B. Moulton, V. Kravtsov and M. J. Zaworotko, J. Am. Chem. Soc., 2002, 124, 9990-9991.

- 12 J. Bernstein, R. E. Davis, L. Shimoni and N. L. Chang, Angew. Chem., Int. Ed. Engl., 1995, 34, 1555-1573.
- 13 S. Jeong, D. Kim and O.-S. Jung, Cryst. Growth Des., 2022, 22, 3245-3251.
- 14 A. Karmakar, A. Paul and A. J. Pombeiro, CrystEngComm, 2017, 19, 4666-4695.
- 15 H. Li, M. Eddaoudi, M. O'Keeffe and O. M. Yaghi, Nature, 1999, 402, 276-279.
- 16 H. Moon, S. W. Lim, D. Kim, O.-S. Jung and Y.-A. Lee, CrystEngComm, 2021, 23, 1272-1280.
- 17 M. Thommes, K. Kaneko, A. V. Neimark, J. P. Olivier, F. Rodriguez-Reinoso, J. Rouquerol and K. S. Sing, Pure Appl. Chem., 2015, 87, 1051-1069.
- 18 D. Kim, G. Kim, J. Han and O. S. Jung, Bull. Korean Chem. Soc., 2022, 43, 1019-1031.
- 19 E. Barea, J. A. Navarro, J. M. Salas, N. Masciocchi, S. Galli and A. Sironi, J. Am. Chem. Soc., 2004, 126, 3014-3015.
- 20 L.-X. Cai, D.-N. Yan, P.-M. Cheng, J.-J. Xuan, S.-C. Li, L.-P. Zhou, C.-B. Tian and Q.-F. Sun, J. Am. Chem. Soc., 2021, 143, 2016-2024.
- 21 C. S. Campos-Fernández, B. L. Schottel, H. T. Chifotides, J. K. Bera, J. Bacsa, J. M. Koomen, D. H. Russell and K. R. Dunbar, J. Am. Chem. Soc., 2005, 127, 12909-12923.
- H. Lee, J. Han, D. Kim and O.-S. Jung, Dalton Trans., 2021, 50, 14849-14854.
- 23 Y.-J. Zhang, T. Liu, S. Kanegawa and O. Sato, J. Am. Chem. Soc., 2010, 132, 912-913.
- 24 B. Manna, A. V. Desai and S. K. Ghosh, Dalton Trans., 2016, 45, 4060-4072.
- 25 R.-Q. Zou, J.-R. Li, Y.-B. Xie, R.-H. Zhang and X.-H. Bu, Cryst. Growth Des., 2004, 4, 79-84.
- 26 J. S. Jang, P. H. Borse, J. S. Lee, O.-S. Jung, C.-R. Cho, E. D. Jeong, M. G. Ha, M. S. Won and H. G. Kim, Bull. Korean Chem. Soc., 2009, 30, 1738-1742.
- 27 E. E. Kim and H. W. Wyckoff, J. Mol. Biol., 1991, 218, 449-464.
- 28 S. Lee, H. Lee and O.-S. Jung, Dalton Trans., 2017, 46, 5843-5847.
- 29 K. Nakashima, X. Zhou, G. Kunkel, Z. Zhang, J. M. Deng, R. R. Behringer and B. De Crombrugghe, Cell, 2002, 108,
- 30 M. Park, H. Kim, H. Lee, T. H. Noh and O.-S. Jung, Cryst. Growth Des., 2014, 14, 4461-4467.
- 31 D. R. Rosen, T. Siddique, D. Patterson, D. A. Figlewicz, P. Sapp, A. Hentati, D. Donaldson, J. Goto, J. P. O'Regan and H.-X. Deng, Nature, 1993, 362, 59-62.
- 32 J. W. Shin, K. Eom and D. Moon, J. Synchrotron Radiat., 2016, 23, 369-373.
- 33 Z. Otwinowski and W. Minor, in Methods in enzymology, Elsevier, 1997, vol. 276, pp. 307-326.
- 34 G. M. Sheldrick, SADABS, A Program for Empirical Absorption Correction of Area Detector Data, University of Göttingen, Germany, 1996.
- 35 G. M. Sheldrick, Acta Crystallogr., Sect. C: Struct. Chem., 2015, 71, 3-8.
- 36 A. Spek, J. Appl. Crystallogr., 2003, 36, 7-13.

- CrystEngComm
- 37 V. A. Blatov, IUCr CompComm Newsletter, 2006, vol. 7, p. 4.
- 38 B. Valeur and M. N. Berberan-Santos, Molecular fluorescence: principles and applications, John Wiley & Sons, 2012.
- 39 S.-L. Zheng, M.-L. Tong, X.-L. Yu and X.-M. Chen, J. Chem. Soc., Dalton Trans., 2001, 586-592.
- 40 H. Irving and R. Williams, J. Chem. Soc., 1953, 3192-3205.
- 41 E. Choi, M. Ryu, H. Lee and O.-S. Jung, Dalton Trans., 2017, 46, 4595-4601.
- 42 D. Kim, S. Lee, Y. A. Lee and O.-S. Jung, Transition Met. Chem., 2020, 45, 65-70.
- 43 J. Lee, S. Park, D. Kim, Y.-A. Lee and O.-S. Jung, Inorg. Chem. Front., 2020, 7, 1546-1552.
- 44 L. Yang, Y.-A. Lee and O.-S. Jung, Inorg. Chem. Commun., 2019, 104, 48-53.
- 45 D. Kim, G. Gwak, J. Han, D. Kim and O.-S. Jung, Dalton Trans., 2022, 51, 5810-5817.